

A New AAV10-U7-Mediated Gene Therapy Prolongs Survival and Restores Function in an ALS Mouse Model

Maria Grazia Biferi,¹ Mathilde Cohen-Tannoudji,¹ Ambra Cappelletto,¹ Benoit Giroux,¹ Marianne Roda,¹ Stéphanie Astord,¹ Thibaut Marais,¹ Corinne Bos,¹ Thomas Voit,³ Arnaud Ferry,^{1,2} and Martine Barkats¹

¹Centre of Research in Myology (CRM), Institut de Myologie, Sorbonne Universités, UPMC Univ Paris 06, Inserm UMRS974, GH Pitié Salpêtrière, Paris 75013, France;

²Sorbonne Paris Cité, Université Paris Descartes, Paris 75006, France; ³NIHR GOSH Biomedical Research Centre, Great Ormond Street Institute of Child Health, University College London, and Great Ormond Street Hospital Trust, London WC1N 1EH, UK

One of the most promising therapeutic approaches for familial amyotrophic lateral sclerosis linked to superoxide dismutase 1 (SOD1) is the suppression of toxic mutant SOD1 in the affected tissues. Here, we report an innovative molecular strategy for inducing substantial, widespread, and sustained reduction of mutant human SOD1 (hSOD1) levels throughout the body of SOD1^{G93A} mice, leading to therapeutic effects in animals. Adeno-associated virus serotype rh10 vectors (AAV10) were used to mediate exon skipping of the hSOD1 pre-mRNA by expression of exon-2-targeted antisense sequences embedded in a modified U7 small-nuclear RNA (AAV10-U7-hSOD). Skipping of hSOD1 exon 2 led to the generation of a premature termination codon, inducing production of a deleted transcript that was subsequently degraded by the activation of nonsense-mediated decay. Combined intravenous and intracerebroventricular delivery of AAV10-U7-hSOD increased the survival of SOD1^{G93A} mice injected either at birth or at 50 days of age (by 92% and 58%, respectively) and prevented weight loss and the decline of neuromuscular function. This study reports the effectiveness of an exon-skipping approach in SOD1-ALS mice, supporting the translation of this technology to the treatment of this as yet incurable disease.

INTRODUCTION

Amyotrophic lateral sclerosis (ALS) is the most common adult-onset motor neuron (MN) disorder, characterized by MN degeneration, severe paralysis, and death within 3–5 years after diagnosis.¹ No treatment is currently available, except the drug Riluzole, which offers only a modest survival benefit.² ALS is epidemiologically classified into sporadic (90%–95%) and familial (5%–10%) forms (fALS);³ approximately 12% of fALS cases are caused by over 180 mutations in the superoxide dismutase 1 (*SOD1*) gene, conferring a toxic gain of function to the mutant protein.^{4,5}

Continuous infusion of antisense oligonucleotides (ASOs) into the brain ventricles has been reported as a promising approach to induce significant SOD1 silencing in SOD1^{G93A} rats, but only 10 days of survival extension was achieved with infusion prior to disease onset.⁶ A phase I clinical study using intrathecally delivered ASOs to patients

revealed the absence of serious adverse effects, highlighting the feasibility of this strategy in humans.⁷ Significant SOD1 reduction has also been provided by injection of lentiviral vectors encoding short hairpin RNA targeting human SOD1 (SOD1-shRNA) into the spinal cord parenchyma or multiple muscle groups of SOD1^{G93A} mice.^{8,9} These approaches resulted in a substantial increase in ALS mouse survival, but their clinical applicability remains questionable, due notably to the difficult translation of the vector administration routes to patients.

More recently, the self-complementary adeno-associated virus (AAV) serotype 9 vector was used to deliver SOD1-shRNA in ALS mice after a single intravascular injection.¹⁰ This systemic AAV9 approach was successful in extending the lifespan of SOD1^{G93A} mice injected at birth or later.¹⁰ Another study using AAV serotype rh10 to express artificial microRNA (miRNA) also showed slowing of disease progression and extended survival in SOD1^{G93A} mice intrathecally injected with the vector at 65 days of age.¹¹ These and other^{12,13} recent AAV studies have provided encouraging therapeutic results and the potential of feasible translation to the clinic. However, these approaches have only led to incomplete rescue and better SOD1-silencing approaches in mice are still needed to provide promising treatment options to patients.

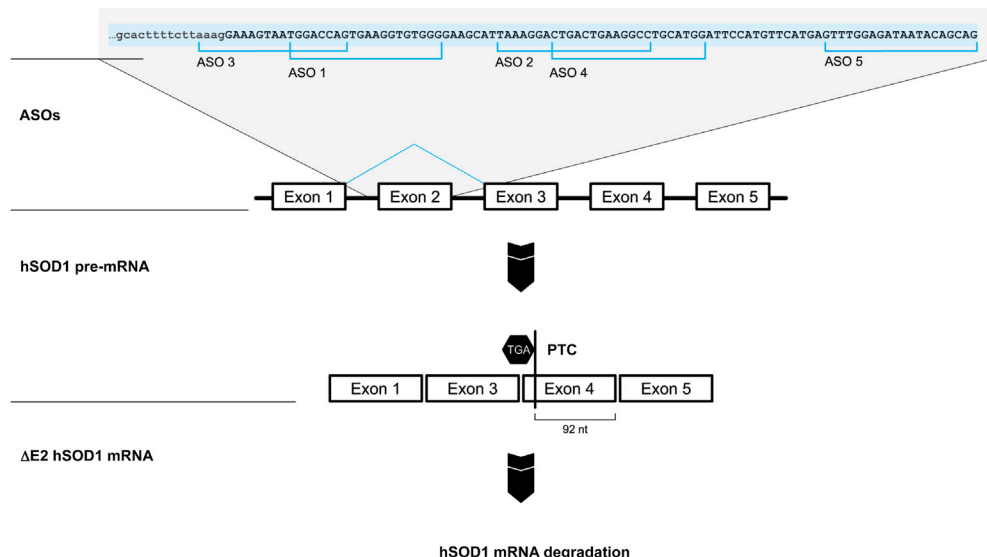
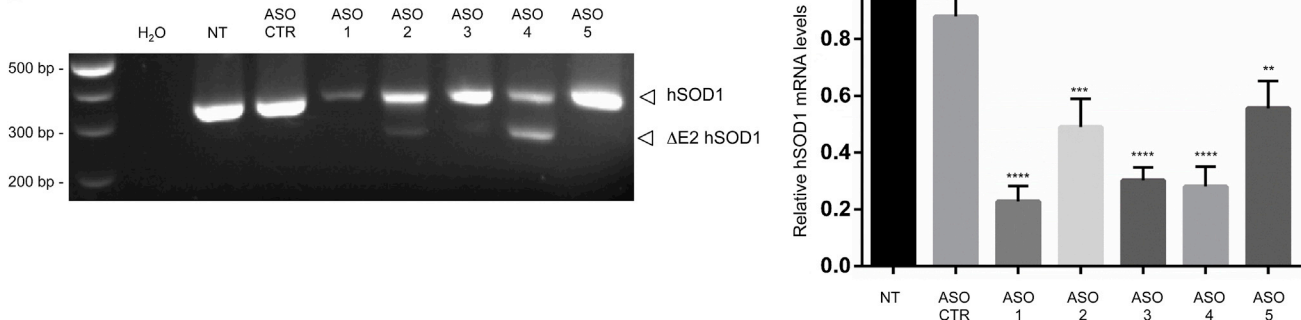
Transcriptional SOD1 silencing can be achieved by skipping of a constitutive SOD1 exon (exon skipping) using ASOs complementary to splicing regulatory elements on the primary transcript. The resulting deleted mRNA, containing a premature termination codon, is then degraded by the endogenous cellular surveillance nonsense-mediated decay pathway.^{14,15}

Here, we report the high therapeutic potential of this exon-skipping strategy in both newborn (P1) and adult (P50) SOD1^{G93A} mice using

Received 15 December 2016; accepted 25 May 2017;
<http://dx.doi.org/10.1016/j.ymthe.2017.05.017>.

Correspondence: Maria Grazia Biferi, Sorbonne Universités, UPMC Univ Paris 06, Inserm UMRS974, Centre of Research in Myology (CRM), Institut de Myologie, GH Pitié Salpêtrière, Paris 75013, France.

E-mail: mg.biferi@institut-myologie.org

A**B****Figure 1. hSOD1 Exon Skipping Reduces mRNA Levels In Vitro**

(A) Schematic representation of E2 skipping in the hSOD1 pre-mRNA induced by specific antisense oligonucleotides (hSOD1-ASO1 to 5). The 9,310-bp hSOD1 gene (Gene ID 6647) comprises five exons separated by four introns, encoding a 153-aa protein. E2 skipping leads to the formation of a premature termination codon (PTC) in exon 4 of the hSOD1-skipped mRNA (ΔE2 hSOD1), 92 nt upstream of the last exon/exon junction (exon 4-exon 5), inducing its degradation by nonsense-mediated decay (NMD) activation. (B) Semiquantitative RT-PCR analysis of HEK293T cells transfected with the five hSOD1-ASOs, showing ΔE2 hSOD1 mRNA production. H₂O, non-transfected cells (NT), and a scrambled control (ASO-CTR) were used as negative controls. Arrowheads indicate full-length (355 bp) and ΔE2 (258 bp) hSOD1 mRNA forms (the shown gel is one replicate of the experiment shown in Figure S1B). The bar graph on the right represents results of qRT-PCR analysis of full-length hSOD1 mRNA expression levels from another set of ASO-transfected HEK293T cells. hSOD1 mRNA was amplified using a specific probe mapping within exon 1-2 of the human SOD1 gene. Results correspond to the percent reduction of full-length hSOD1 mRNA induced by the different ASOs relative to NT. Data are expressed as the mean ± SEM of four independent transfection experiments. Differences between groups were analyzed by one-way ANOVA analysis, followed by Tukey's post hoc test (**p < 0.01; ***p < 0.001; ****p < 0.0001).

the administration of ASOs against mutant human SOD1 (hSOD1) inserted in an AAV10-U7 vector (AAV10-U7-hSOD1). The AAV vector was co-injected into the central nervous system and the peripheral organs, combining intravenous (i.v.) and intracerebroventricular (i.c.v.) injections. This gene therapy approach induced efficient hSOD1 exon skipping in the spinal cord, resulting in a large reduction of hSOD1 mRNA and protein levels. SOD1^{G93A} mice survival was prolonged, with a mean increase in life expectancy of 92% and 58% for mice injected either at birth or 50 days of age, respectively. Disease onset was also delayed by 95 and 63 days, respectively, relative to un-

treated mice. Finally, AAV10-U7-hSOD1 delivery prevented weight loss and preserved motor function and skeletal muscle force.

RESULTS

Specific Antisense Sequences Promote hSOD1 Exon Skipping In Vitro

We rationally designed five steric, blocking RNA-based ASOs that masked the splicing acceptor site (SA) in intron 1 or exonic splicing enhancer sequences (ESEs)¹⁶ in exon 2 (E2) to promote efficient E2 skipping (Figures 1A and S1A). Skipping of hSOD1 E2 generates a

frameshift in the mRNA transcript, with production of a premature stop codon in exon 4 (E4), 92 nt upstream of the E4-E5 junction (Figure 1A). The deleted transcript (Δ E2 hSOD1) is a likely substrate for the endogenous cellular surveillance nonsense-mediated decay pathway and is subsequently degraded because the premature stop codon is located greater than 55 nt upstream of the last exon-exon junction.¹⁷

The ASOs were chemically modified (2'-O-methyl phosphorothioate [2'OMePS]) to increase their stability, resist nuclease and RNase H degradation,¹⁸ and their ability to promote E2 skipping was evaluated (hSOD1-ASO). A scrambled fluorescently (FAM)-labeled ASO was used as control (ASO-CTR). After ASO transfection into HEK293T cells, RT-PCR analysis revealed a 258-nt band corresponding to the Δ E2 hSOD1 mRNA variant in the samples transfected with hSOD1-ASO and a 355-nt product corresponding to the complete hSOD1 mRNA in all samples (Figures S1B and S1C). Although all ASOs resulted in a substantial reduction of hSOD1 mRNA levels relative to non-transfected cells, ASO1 and ASO4 showed the highest efficiency (Figure 1B). These two ASOs, targeting different ESE regions in E2, were both used in the following studies to expand the masked sequence and maximize steric hindrance to splicing factors.

AAV10-U7-Mediated Delivery of Antisense Sequences in SOD1^{G93A} Mice Reduces hSOD1 Protein and mRNA Levels

We sub-cloned the two AS sequences corresponding to ASO1 and ASO4 into the optimized U7-snRNA cassette (U7-AS-1/AS-4), previously described by Schumperli et al.,¹⁹ to protect them from degradation. The embedding of ASOs into the U7snRNP particle has been reported to improve their nuclear entry and incorporation into the spliceosome and increase their stability in vivo.^{19,20} We then engineered the U7-AS-1/AS-4 cassette or a control AS, previously tested in vivo,²¹ into the AAV backbone, and the corresponding AAV10 vectors were produced (AAV10-U7-hSOD1 or AAV10-U7-CTR) (Figure 2A).

We locally injected the AAV10-U7-hSOD1 or the AAV10-U7-CTR vectors (4.7×10^{12} viral genome [vg]/kg, two sites, 4.8×10^{10} per site in 5 μ L) into the lumbar spinal cord of 50-day-old SOD1^{G93A} mice to analyze the efficiency of AAV10-U7-hSOD1 in reducing hSOD1 mRNA and protein levels in vivo. As expected, we found the Δ E2 hSOD1 mRNA variant in the spinal cords of AAV10-U7-hSOD1-injected animals 1 month after injection, with a more than 80% reduction of full-length hSOD1 mRNA for each injected mouse (Figure 2B) and a 70% average reduction in hSOD1 protein relative to AAV10-U7-CTR-injected animals (Figure 2C). Due to the high degree of homology between hSOD1 and murine SOD1 sequences, ASOs were designed to be human specific, with AS-1/AS-4 presenting a total of ten mismatches to the mouse SOD1 mRNA (Figure S2A). Accordingly, the endogenous SOD1 protein levels were unchanged in all injected animals, confirming the specificity of AAV10-U7-hSOD1 for the hSOD1 form (Figures S2B and S2C).

Co-i.v./i.c.v. Administration of AAV10-U7-hSOD1 in Newborn SOD1^{G93A} Mice Prolongs Survival and Delays Disease Onset

To test the therapeutic efficacy of hSOD1 exon skipping, we injected SOD1^{G93A} mice on postnatal day 1 (PND1) with 4.5×10^{14} vg/kg of AAV10-U7-hSOD1 ($n = 15$) or AAV10-U7-CTR vectors ($n = 17$) co-injected into the temporal vein (i.v., 4×10^{14} vg/kg) and lateral ventricles (i.c.v., 5×10^{13} vg/kg) (co-i.v./i.c.v.) (Figure 3A). All AAV10-U7-hSOD1-injected SOD1^{G93A} mice survived substantially longer than did non-injected (NI) ($n = 12$) or AAV10-U7-CTR-injected mice (239 days versus 118 days or 125 days, respectively; $p < 0.0001$), for an extension of the median lifespan of 121 and 114 days, respectively. No statistically significant difference was found between the lifespans of AAV10-U7-CTR-injected and NI mice (Figure 3B).

The mean lifespan of AAV10-U7-hSOD1-injected mice was 95% and 92% longer than that of NI or AAV10-U7-CTR-injected mice, respectively (Figure 3C).

AAV10-U7-hSOD1 delivery also slowed the weight loss observed in NI SOD1^{G93A} mice at the end stage (23.9 ± 1.1 g versus 20.5 ± 0.9 g at 17 weeks, $p < 0.05$) (Figure 3D), and, importantly, AAV10-U7-hSOD1-injected mice gained weight until \sim 25 weeks of age, at which point weight reached a plateau. The weights of AAV10-treated SOD1^{G93A} mice and wild-type (WT) mice were statistically significantly different at 25 weeks of age (25.6 ± 1.4 g versus 30.7 ± 1.4 g, respectively; $p < 0.05$) (Figure 3D).

AAV10-U7-hSOD1 delivery significantly delayed disease onset, based on the age of peak body weight, by \sim 102 and 95 days relative to NI and AAV10-U7-CTR-injected mice, respectively (199.5 days versus 97.5 days and 104.5 days; $p < 0.0001$) (Figure 3E). No statistically significant difference was observed between disease onset of AAV10-U7-CTR-injected and NI mice (Figure 3E). The mean disease progression, defined as the time from disease onset to death, was significantly delayed by 14 days in AAV10-U7-hSOD1-injected mice (36.6 ± 4.9 days) relative to NI mice (23.1 ± 1.7 days, $p < 0.05$) and AAV10-U7-CTR-injected mice (22.8 ± 3.7 days, $p < 0.05$) (Figure 3F).

Co-i.v./i.c.v. Administration of AAV10-U7-hSOD1 in Newborn SOD1^{G93A} Mice Reduces hSOD1 Levels and Preserves Pathological Signs

We analyzed the efficacy of E2 skipping for the silencing of hSOD1 in the spinal cords of SOD1^{G93A} mice, co-i.v./i.c.v. injected at birth, both at 112 days of age ($n = 3$) and at the end stage ($n = 3$) (Figure S3). We observed a significant reduction of full-length hSOD1 mRNA at both ages relative to those of NI mice (76% and 65% reduction at 112 days of age and end stage, respectively; $p < 0.0001$) and AAV10-U7-CTR-injected mice (77% and 66% reduction at 112 days of age and end stage, respectively; $p < 0.0001$) (Figure S3A). The levels of hSOD1 protein were also reduced by 71% and 66% in the spinal cord of AAV10-U7-hSOD1-injected SOD1^{G93A} mice at 112 days of age relative to those of NI mice and AAV10-U7-CTR-injected mice,

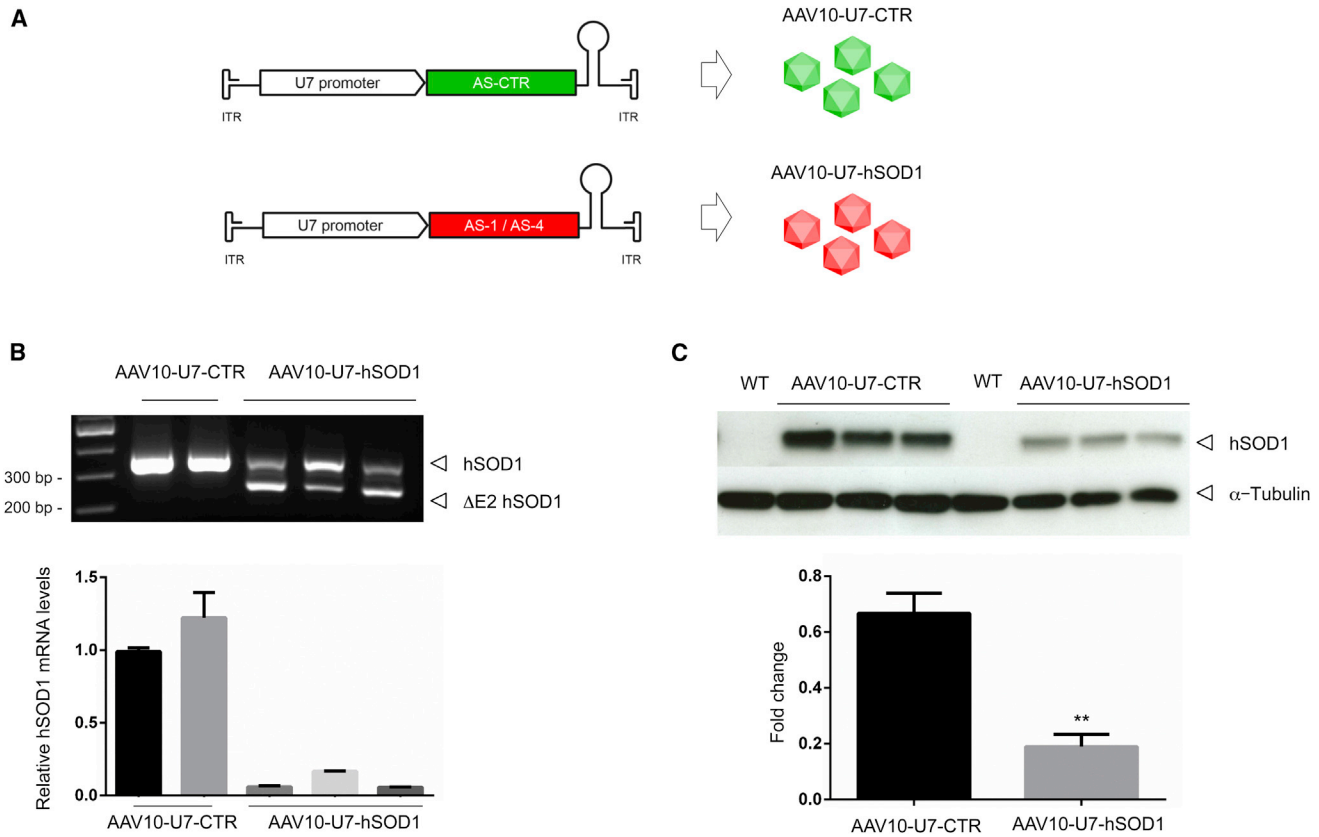


Figure 2. AAV-U7-Mediated hSOD1 Exon Skipping Reduces mRNA and Protein Levels In Vivo

(A) Design of the AAV vectors used to target hSOD1 (AAV10-U7-hSOD1) or control (AAV10-U7-CTR) sequences. The antisense sequences (ASs) corresponding to ASO1 and ASO4 were embedded into the optimized human U7 small nuclear RNA (snRNA)^{19,20} and cloned between two AAV inverted terminal repeats (ITRs). (B) The upper panel corresponds to a semiquantitative RT-PCR analysis of mRNA extracted from the spinal cord (SC) of SOD1^{G93A} mice, in which the lumbar SC was injected with 4.7×10^{12} vg/kg of AAV10-U7-hSOD1 ($n = 3$) or AAV10-U7-CTR ($n = 2$). The lower panel shows results of the corresponding qRT-PCR analysis, showing lower levels of full-length hSOD1 mRNA in SC from AAV10-U7-hSOD1-injected mice than AAV10-U7-CTR-injected controls. Data are expressed as the mean \pm SEM. (C) Western blot (WB) analysis of hSOD1 protein expression in SOD1^{G93A} mice, in which the SC was injected with AAV10-U7-hSOD1 ($n = 3$) or AAV10-U7-CTR ($n = 3$) (4.7×10^{12} vg/kg). Antibody specificity for the human form of SOD1 was demonstrated by the absence of signal in protein extracts from WT mice. α -Tubulin was used as a loading control. The lower panel corresponds to the densitometric analysis of WB results, showing the significant reduction of hSOD1 levels in the AAV10-U7-hSOD1-injected SCs. Values are expressed as the mean \pm SEM, and differences between groups were analyzed by the Student's t test (** $p < 0.01$).

respectively ($p < 0.05$). However, we detected no significant difference in hSOD1 protein levels at the end stage among AAV10-U7-hSOD1-injected, AAV10-U7-CTR-injected, or NI animals, despite the significant decrease of mRNA, suggesting progressive accumulation of residual amounts of mutant hSOD1 protein in the treated mice (Figure S3B).

We investigated the possible production of a protein from the truncated SOD1 mRNA after the prolonged expression of AAV10-U7-hSOD1 in the spinal cords of SOD1^{G93A} mice injected at birth ($n = 4$) (Figure S4). If the ΔE2 hSOD1 mRNA is translated into protein, the latter will have a different amino acid sequence downstream of the end of exon 1 and will be made of 55 amino acids. Using the hSOD1-specific antibody, recognizing the N-terminal portion of the hSOD1

protein, we detected no protein signal at the presumed size of the truncated protein (6.05 kDa) (Figure S4A). As expected, with the same antibody, we confirmed that the levels of the hSOD1 protein were reduced by 76% in AAV10-U7-hSOD1-injected SOD1^{G93A} mice relative to those of NI mice at 112 days of age ($p < 0.0001$) (Figure S4B).

Double-immunofluorescence analysis of spinal cord sections using antibodies against hSOD1 and either choline acetyl transferase (ChAT) (a marker of MNs) or glial fibrillary acid protein (GFAP) (a marker of astrocytes) confirmed the reduction of hSOD1 protein levels in individual MNs from AAV10-U7-hSOD1-injected mice at 112 days of age, but also in astrocytes, another cell type involved in ALS pathogenesis²² (Figure S5).

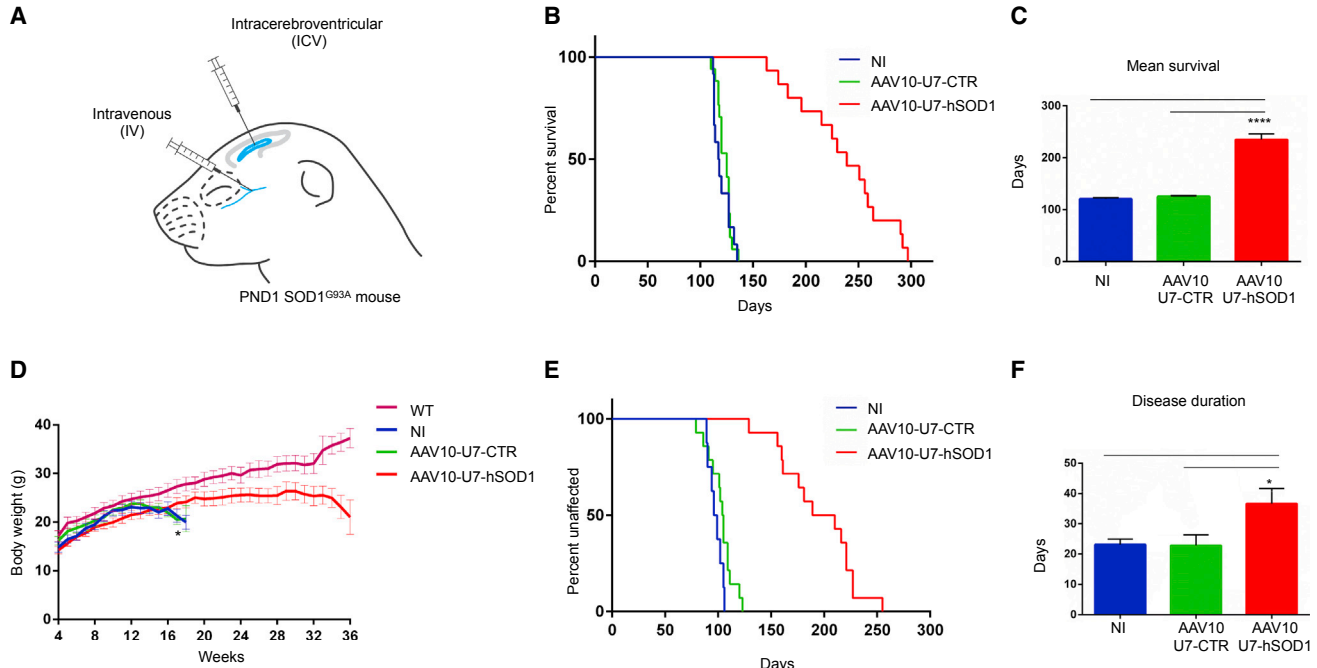


Figure 3. Combined i.v./i.c.v. Delivery of AAV10-U7-hSOD1 Prolongs Survival in Neonatal SOD1^{G93A} Mice

(A) Schematic representation of AAV10 delivery into the temporal vein (i.v.) and lateral ventricles (i.c.v.) (co-i.v./i.c.v.) of SOD1^{G93A} mice on PND1. The mice were injected with a total dose of 4.5×10^{14} vg/kg of AAV10-U7-hSOD1 or AAV10-U7-CTR vectors (i.v., 4×10^{14} vg/kg, and i.c.v., 5×10^{13} vg/kg). (B) Kaplan-Meier survival curves of SOD1^{G93A} mice co-i.v./i.c.v. injected with either AAV10-U7-SOD1 (red, n = 15) or AAV10-U7-CTR (green, n = 17) and NI mice (blue, n = 12). Differences between the curves were analyzed using the log rank Mantel-Cox test, showing a significant difference between AAV10-U7-SOD1-injected mice and either AAV10-U7-CTR-injected or NI mice ($***p < 0.0001$). (C) Bar graph indicating a significant difference between the mean survival of AAV10-U7-SOD1- and either AAV10-U7-CTR-injected mice or NI mice (235.6 ± 11 days versus 120.1 ± 2.3 days and 122.9 ± 1.6 days, respectively). Data are expressed as the mean \pm SEM, and differences between groups were analyzed by one-way ANOVA analysis followed by Tukey's post hoc test ($***p < 0.0001$). (D) Body weight curves of AAV10-U7-hSOD1-injected SOD1^{G93A} mice (red) compared to AAV10-U7-CTR-injected SOD1^{G93A} mice (green), NI SOD1^{G93A} mice (blue), and WT mice (pink) (n = 8 in each sex-balanced group, Student's t test, *p < 0.05). (E) Kaplan-Meier curves showing the significant delay in median disease onset (based on the age at body-weight peak) in mice injected with either AAV10-U7-hSOD1 (red, n = 14) relative to NI mice (blue, n = 8) and AAV10-U7-CTR-injected mice (green, n = 14). Differences between the curves were analyzed by the log rank Mantel-Cox test ($***p < 0.0001$). (F) Mean duration of disease of mice injected with either AAV10-U7-hSOD1 (red, n = 14) or AAV10-U7-CTR (green, n = 14) and of NI mice (blue, n = 8), showing the significant extension of disease duration in the AAV10-U7-hSOD1-treated animals. Results are expressed as the mean \pm SEM, and the differences between groups were determined by one-way ANOVA, followed by Tukey's post hoc test (*p < 0.05).

Skeletal muscles have also been shown to be involved in the pathogenesis of ALS;²³ thus, we further quantified the level of hSOD1 silencing in the *triceps* muscle. We found 40% lower hSOD1 mRNA levels in the *triceps* muscles of AAV10-U7-hSOD1-injected SOD1^{G93A} mice than in those of NI or AAV10-U7-CTR-injected mice (n = 3; p < 0.01) (Figure S6A).

We then quantified the main neuropathological features of ALS observed in SOD1^{G93A} mice, such as MN loss, astrogliosis, and microglia activation.²⁴ AAV10-U7-hSOD1 delivery significantly prevented ChAT⁺ MN degeneration at 112 days of age (11.8 ± 0.4 versus 9.7 ± 0.2 and 8.7 ± 0.2 , for NI and AAV10-U7-CTR delivery, respectively; p < 0.0001) (Figures 4A and 4B, upper panels), reduced the intensity of GFAP fluorescence (astrocytosis) (27.7 ± 1.8 versus 54.0 ± 1.9 and 49.5 ± 2.3 for NI and AAV10-U7-CTR, respectively; p < 0.001) (Figures 4A and 4B, middle panels), and decreased the number of ionized calcium-binding adaptor molecule 1 positive (Iba1⁺) micro-

glial cells (38.3 ± 2.2 versus 151.1 ± 6.0 and 138.5 ± 4.7 for NI and AAV10-U7-CTR, respectively; p < 0.0001) (Figures 4A and 4B, lower panels).

We assessed skeletal muscle denervation by analyzing the occupancy of neuromuscular junctions (NMJs) in AAV10-U7-hSOD1-injected SOD1^{G93A} mice, NI SOD1^{G93A} mice, and WT mice at 112 days by double staining of the *extensor digitorum longus* (EDL) muscles for bungarotoxin (BTX) (binding to the nicotinic acetylcholine receptor of NMJ) and neurofilament (NF) (fibrillar component of the axons) (Figure 4C). After AAV10-U7-hSOD1 injection, $64.0 \pm 3.2\%$ of endplates were innervated in SOD1^{G93A} mice, with no significant difference to WT mice ($80.3 \pm 7.0\%$) (Figure 4D, left panel). Conversely, NI SOD1^{G93A} mice presented $31.5 \pm 8.5\%$ of innervated endplates and were significantly different from both AAV-treated and WT mice (p < 0.05 and p < 0.01; respectively) (Figure 4D, left panel). Endplates'

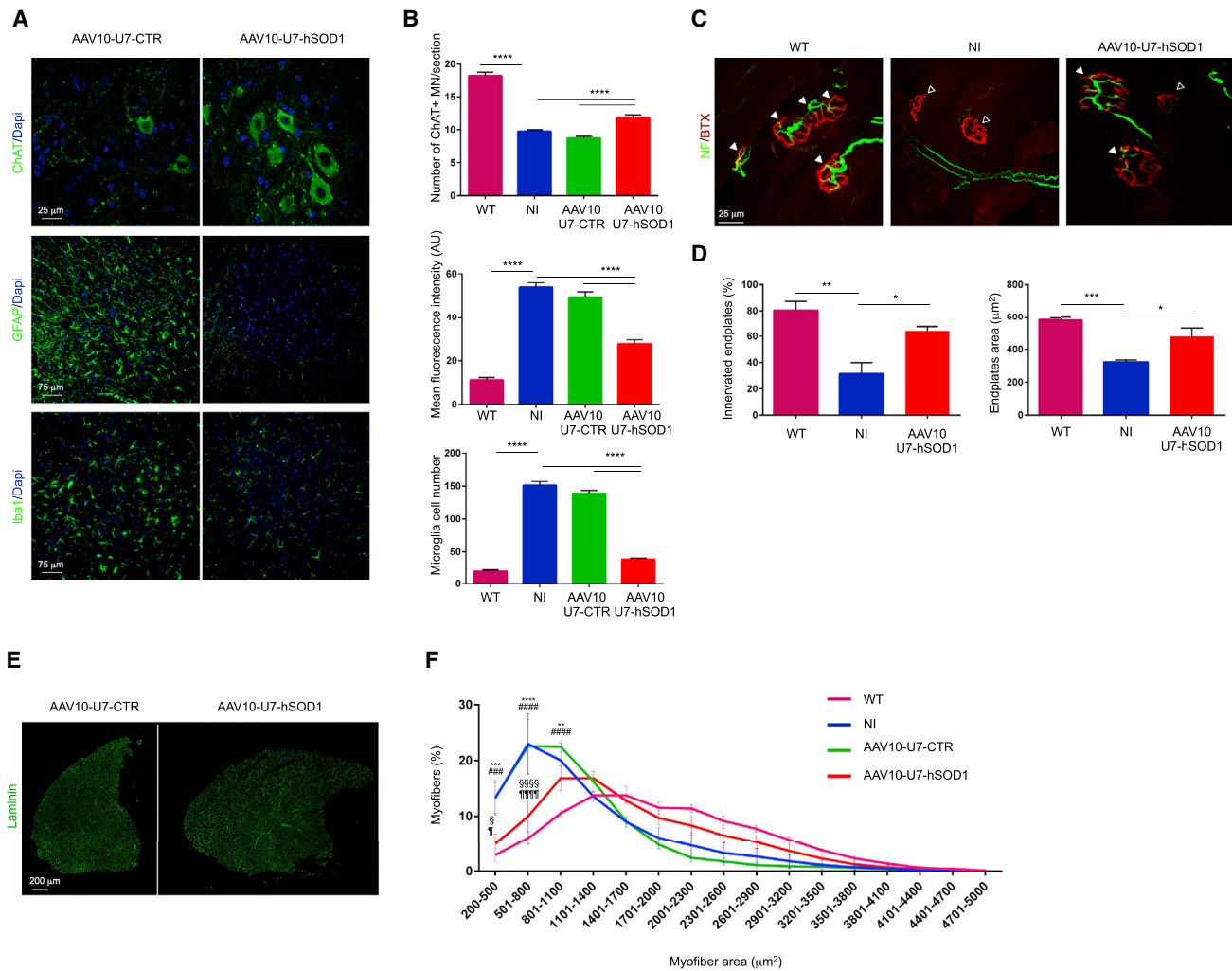


Figure 4. AAV10-U7-hSOD1 Injection in Newborn SOD1^{G93A} Mice Rescues the ALS Phenotype

(A) Representative transverse sections of the ventral horn of the lumbar spinal cord from SOD1^{G93A} mice injected at birth with AAV10-U7-hSOD1 or AAV10-U7-CTR and processed for immunofluorescence at 112 days of age using anti-ChAT (upper panels), anti-GFAP (middle panels), or anti-Iba1 (lower panels) antibodies. Scale bar, 25 or 75 μm , as indicated. (B) Quantitative analysis of the number of ChAT-positive motor neurons (upper panel, n = 6, 50 sections per mouse), the mean fluorescence intensity of GFAP immunostaining (middle panel, n = 6, three sections per mouse), and the number of Iba1-positive cells (lower panel, n = 6, three sections per mouse) in AAV10-U7-hSOD1- or AAV10-U7-CTR-injected SOD1^{G93A} mice, NI SOD1^{G93A} mice, and WT mice. Data are expressed as the mean \pm SEM. ***p < 0.0001, one-way ANOVA followed by Tukey's post hoc test. (C) Representative NMJ of the EDL muscles from WT mice and SOD1^{G93A} mice, injected at birth with AAV10-U7-hSOD1 or NI, and analyzed for whole mount immunofluorescence at 112 days. Endplates were identified by 594-conjugated BTX (red); terminal axons were identified by anti-NF antibody (green). Full arrowheads indicate innervated endplates; empty arrowheads indicate denervated endplates. Scale bar, 25 μm . (D) Quantification of innervated endplates (left panel) and endplate areas (right panel) in WT, AAV10-U7-hSOD1-injected SOD1^{G93A} mice, or NI SOD1^{G93A} mice (n = 4; \sim 50 BTX-positive endplates per animal were randomly chosen and analyzed). Data are expressed as the mean \pm SEM. *p < 0.05; **p < 0.01; ***p < 0.001; one-way ANOVA followed by Tukey's post hoc test. (E) Representative transverse sections of the TA muscle from AAV10-U7-hSOD1- or AAV10-U7-CTR-injected SOD1^{G93A} mice processed for anti-laminin immunofluorescence at 112 days of age. Scale bar, 200 μm . (F) Frequency distribution curves of myofiber areas in the TA muscle of AAV10-U7-hSOD1- or AAV10-U7-CTR-injected SOD1^{G93A} mice, NI mice, and WT mice. N = 3 mice per group. Data are expressed as the mean \pm SEM. **p < 0.01, ***p < 0.001, and ****p < 0.0001 for NI compared to WT; #p < 0.001 and #####p < 0.0001 for AAV10-U7-CTR compared to WT; ^p < 0.05 and ^###p < 0.0001 for AAV10-U7-hSOD1 compared to NI; ^p < 0.05 and ^###p < 0.0001 for AAV10-U7-hSOD1 compared to AAV10-U7-CTR; two-way ANOVA followed by Bonferroni post hoc test (treatment and frequency).

surface was preserved in AAV10-U7-hSOD1-injected SOD1^{G93A} mice ($480.5 \pm 50.52 \mu\text{m}^2$) compared with NI and WT animals ($324.3 \pm 12.48 \mu\text{m}^2$, p < 0.05 and $580.3 \pm 17.13 \mu\text{m}^2$) (Figure 4D, right panel).

Furthermore, measurement of *tibialis anterior* (TA) muscle sections showed a 53% greater mean section area in AAV10-U7-hSOD1-treated mice ($4.6 \times 10^6 \pm 0.3 \times 10^6 \mu\text{m}^2$) than in either AAV10-U7-CTR-injected ($3.0 \times 10^6 \pm 0.2 \times 10^6 \mu\text{m}^2$; p < 0.05) or NI

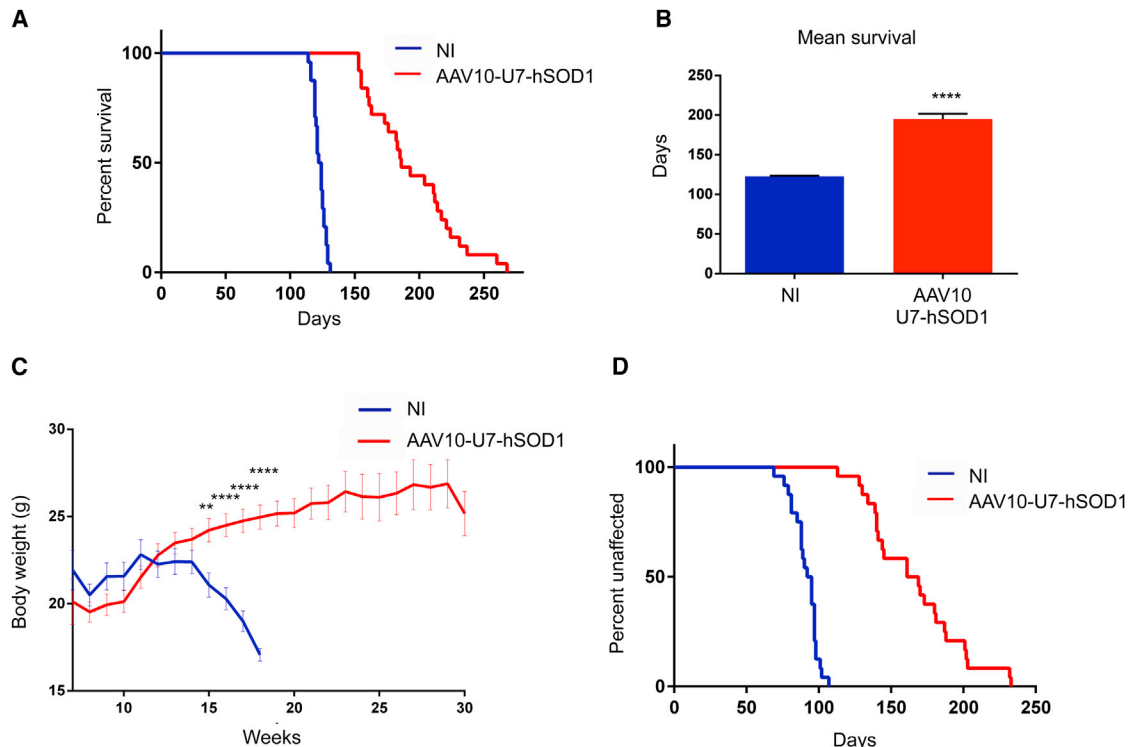


Figure 5. Combined i.v./i.c.v. Injection of AAV10-U7-hSOD1 Rescues Survival of Adult SOD1^{G93A} Mice

(A) Kaplan-Meier survival curves of SOD1^{G93A} mice co-i.v./i.c.v. injected at PND50 with AAV10-U7-SOD1 (4.5×10^{14} vg/kg total, n = 25) or NI (n = 24), sex-balanced group. The median lifespan was significantly longer for mice treated with AAV10-U7-hSOD1 than for NI mice (186 days versus 123 days; ****p < 0.0001, log rank Mantel-Cox test). (B) Comparison of the mean survival of AAV10-U7-SOD1-injected (red, n = 25) and NI mice (blue, n = 24) (195 ± 6.7 days versus 122.8 ± 0.9 days). Data are expressed as the mean \pm SEM, ****p < 0.0001, Student's t test. (C) Comparison of the body weight curves of AAV10-U7-hSOD1-injected and NI SOD1^{G93A} mice (n = 24 per sex-balanced group). **p < 0.01; ***p < 0.0001, Student's t test. (D) Kaplan-Meier curves illustrating the onset of disease, defined by the age at the peak body weight, for AAV10-U7-hSOD1-injected (red, n = 24) and NI (blue, n = 24) SOD1^{G93A} mice. The median time of disease onset was significantly delayed for the AAV10-U7-hSOD1-injected mice relative to that of NI mice. Differences between the curves were analyzed by the log rank Mantel-Cox test; ****p < 0.0001.

($3.0 \times 10^6 \pm 0.4 \times 10^6 \mu\text{m}^2$; p < 0.05) mice (Figure 4E). The frequency distribution curves of myofiber diameters, determined by anti-laminin immunofluorescence analysis, revealed a shift toward larger fibers in the TA of AAV10-U7-hSOD1-treated mice relative to controls, with a distribution of small caliber fibers similar to that of WT mice (Figure 4F). The alteration in muscle fiber composition induced by denervation²⁵ was also prevented in the AAV10-U7-hSOD1-treated SOD1^{G93A} mice, as revealed by immunostaining for type IIa myosin heavy chain (MHC-IIa), representing the myosin isoform predominantly expressed in TA fast fibers of SOD1^{G93A} mice, compared to type IIb or IIx MHC isoforms.²⁶ The treatment significantly reduced the number of MHC-IIa-positive fibers ($7.8 \pm 0.9\%$ of total fibers) relative to NI and AAV10-U7-CTL-injected mice ($13.0 \pm 1.2\%$ and $13.0 \pm 1.3\%$, respectively) (Figure S6B).

AAV10-U7-hSOD1-Mediated Gene Therapy Rescues 50-Day-Old ALS Mice Survival

We further investigated the potential therapeutic effects of AAV10-U7-hSOD1-mediated SOD1 silencing in adult mice, when muscle denerva-

tion is already present,^{27,28} by co-i.v./i.c.v. injecting 50-day-old SOD1^{G93A} mice (n = 25) with the vector (i.v., 4.2×10^{14} vg/kg and 3.0×10^{13} vg/kg, respectively). The median survival of AAV10-U7-hSOD1-treated mice was extended by 63 days relative to NI controls (n = 24) (186 days versus 123 days; p < 0.0001) (Figure 5A), and the mean life expectancy was extended by 58% (195.0 ± 6.7 days versus 122.8 ± 0.9 days; p < 0.0001) (Figure 5B). AAV10-U7-hSOD1 delivery also significantly prevented weight loss starting at 15 weeks of age in NI SOD1^{G93A} mice (24.2 ± 0.6 g versus 21.0 ± 0.6 g, p < 0.01) (Figure 5C). Disease onset was delayed by 71.5 days in the AAV10-U7-hSOD1-injected mice relative to the NI mice (165.0 days versus 93.5 days; p < 0.0001) (Figure 5D). There was no significant increase in the duration of disease progression between AAV10-U7-hSOD1-injected mice and NI mice (31.7 ± 1.8 days and 28.2 ± 3 days, respectively; p = 0.33).

Widespread AAV10-U7-hSOD1-Mediated hSOD1 Suppression Delays Disease Signs in Adult SOD1^{G93A} Mice

We observed a significant reduction of hSOD1 mRNA and protein levels in both the CNS and peripheral organs of mice injected with

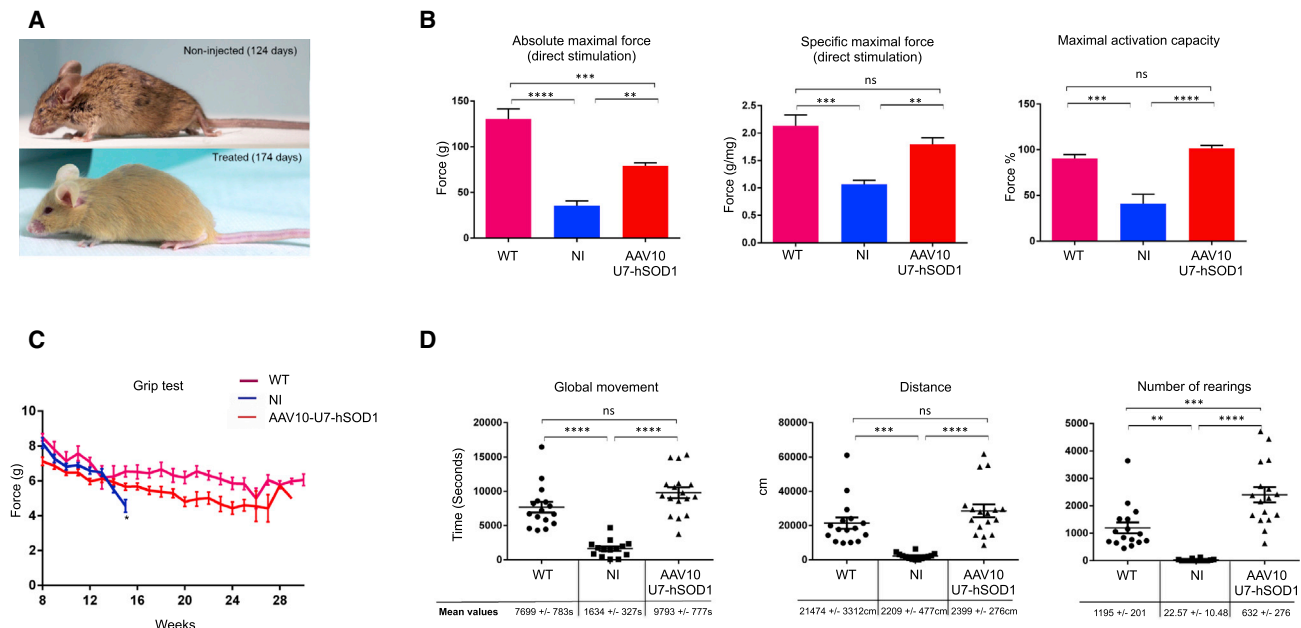


Figure 6. Combined i.v./i.c.v. Injection of AAV10-U7-hSOD1 Preserves Neuromuscular Function in Adult SOD1^{G93A} Mice

(A) Photographs illustrating the phenotype of a NI SOD1^{G93A} mouse at 124 days of age displaying kyphosis, closed eyes, self-grooming defects, and lower limb paralysis (upper panel), and of a 174-day-old AAV10-U7-hSOD1-injected SOD1^{G93A} mouse (whose phenotype was similar to WT mice) (lower panel). (B) Absolute and specific maximal forces in response to muscle stimulation (direct stimulation), and maximal activation capacity that was a functional index of neuromuscular transmission measured in 112-day-old AAV10-U7-hSOD1-injected SOD1^{G93A} mice, age-matched WT mice, and 112-day-old NI SOD1^{G93A} mice ($n = 3$ per group). Data are expressed as the mean \pm SEM. ** $p < 0.01$; *** $p < 0.001$; **** $p < 0.0001$, one-way ANOVA followed by Tukey's post hoc test. (C) Grip strength was assessed twice a week from the day of treatment in injected (red) and NI (blue) SOD1^{G93A} mice ($n = 24$ per group) as well as in age- and sex-matched WT animals (pink, $n = 10$). Data are expressed as the mean per week \pm SEM. The difference between injected and NI mice was statistically significant at 15 weeks of age (* $p < 0.05$, Student's t test). (D) Spontaneous motor activity monitored during 12 hr overnight in AAV10-U7-hSOD1-injected ($n = 17$), NI SOD1^{G93A} mice ($n = 14$), and WT mice ($n = 16$) (sex-balanced groups) at 120 days of age. The analyzed parameters were the time spent moving (left panel), distance covered (middle panel) (cm), and number of rearings (right panel). Individual data for WT (circles), NI (squares), and AAV10-U7-hSOD1 (triangles) are indicated, as well as the mean values \pm SEM. * $p < 0.05$; ** $p < 0.01$; *** $p < 0.001$; **** $p < 0.0001$, one-way ANOVA followed by Tukey's post hoc test.

AAV10-U7-hSOD1 at the age of 50 days ($n = 3$) relative to NI mice ($n = 3$) (Figure S7), similar to the results of SOD1^{G93A} mice injected at birth and confirming the consistent targeting of multiple tissues. Histopathological analysis of the spinal cord and TA muscle in SOD1^{G93A} mice injected at the age of 50 days also showed 35% more MNs relative to age-matched NI mice (Figure S8A) and a total area and frequency distribution of the myofiber area in the TA muscle that was similar to that of WT mice (Figure S8C).

The overall phenotype of the treated SOD1^{G93A} mice was considerably improved relative to that of NI mice, as illustrated in Figure 6A, with 36% of SOD1^{G93A}-treated mice never showing signs of hind-limb paralysis. When present, the duration of paralysis, calculated as the time from muscle rigidity onset to death, was significantly extended by the treatment (16.7 ± 2.7 days versus 10.0 ± 1.4 days in NI; $p < 0.05$; Student's t test), although there was no increase in disease duration in the AAV10-U7-hSOD1-injected mice, suggesting a potential beneficial effect of the treatment on muscle innervation.⁹ This was confirmed by the observation of NMJ protection in the *gastrocnemius* muscle of SOD1^{G93A} mice injected with AAV10-U7-hSOD1 at 50 days relative to NI SOD1^{G93A} mice ($48.0 \pm 2.5\%$ versus

$16.0 \pm 2.0\%$ of innervated endplates; $p < 0.001$; Student's t test) (Figure S8B).

A further comparison of the contractile properties of the TA muscle from AAV10-U7-hSOD1-injected and NI mice confirmed the impact of hSOD1 silencing on neuromuscular function. The absolute maximal force generated during isometric TA muscle contraction after direct stimulation of the TA muscle of 112-day-old AAV10-injected mice was double that of NI mice (79.2 ± 3.1 g versus 35.6 ± 5.1 g; respectively, $p < 0.01$), but still lower than that of WT mice (130.5 ± 10.0 g, $p < 0.001$) (Figure 6B, left panel). However, when the absolute force was normalized to muscle mass, the specific maximal force was 69% greater in treated than in NI mice (1.8 ± 0.1 g versus 1.1 ± 0.1 g; $p < 0.01$) with no statistically significant difference from that of WT mice (2.1 ± 0.1 g) (Figure 6B, middle panel). Moreover, the maximal activation capacity of the TA muscle (defined as the percentage of force generated in response to sciatic nerve stimulation relative to muscle stimulation) was more than 100% higher in treated mice than in NI controls (101.6 ± 3.1 versus 41.2 ± 10.0 ; $p < 0.0001$), and was not different from that of WT mice (90.3 ± 11.0) (Figure 6B, right panel), demonstrating the functional maintenance of neuromuscular transmission and functional force generation.

We confirmed the beneficial effect of AAV10-U7-hSOD1 on neuromuscular function by analyzing muscle strength in a grip test, showing the maintenance of muscle force over the lifespan of treated mice that had a significantly greater grip force than did NI mice (5.6 ± 0.2 g versus 4.5 ± 0.3 g, $p < 0.05$) and no statistically significant difference from that of WT mice (6.5 ± 0.3 , NS), at 15 weeks of age (Figure 6C). The analysis of spontaneous motor activity in an actimeter also showed the complete rescue of the overall activity of the treated mice, which was significantly greater than that of NI mice and similar to that of WT mice (Figure 6D; Movie S1). In contrast, motor coordination of the SOD1^{G93A} mice measured by the rotarod test was only partially restored by AAV10-U7-hSOD1 delivery because the latency to fall of the injected mice was still significantly higher than that of NI mice at 15 weeks of age (31.0 ± 3.3 s versus 21.4 ± 2.2 s, $p < 0.05$), but remained lower than that of WT mice (59.2 ± 2.6 s; $p < 0.0001$) (Figure S9).

DISCUSSION

In summary, we showed the efficacy of a new gene therapy approach for silencing mutant hSOD1 expression throughout the body of SOD1^{G93A} mice by AAV10 delivery of a U7-AS construct that functionally skips exon 2 of hSOD1 out of frame. Survival and the results of functional tests exceeded any reported results from previous hSOD1-silencing approaches. This increased effect is likely due to the combination of a more efficient gene-silencing method and the targeting of both central and peripheral tissues.

The reduction in mutant SOD1 levels induced by AAV10-mediated exon skipping was much greater than those reported in previous studies using AAV9- or AAV10-mediated RNA interference,^{10,11,13} with a nearly 70% reduction of hSOD1 protein levels in the spinal cord.

This effect is most likely due to the use of U7-delivered antisense molecules, acting at the pre-mRNA level and hampering the formation of a full-length hSOD1 mRNA and its toxic product. To establish whether the described exon-skipping approach outperforms RNA-interference techniques (artificial miRNA or short hairpin RNA), a direct comparison of the different molecular strategies tested under the same conditions (e.g., same amount of vectors and delivery route) is needed. These studies will be helpful to identify the best method for hSOD1 reduction *in vivo*.

Moreover, co-delivery of the therapeutic vector into the cerebrospinal fluid and bloodstream resulted in efficient SOD1 silencing in tissues known to be involved in SOD1^{G93A}-mediated toxicity, including MNs and glial cells in the spinal cord²⁴ and skeletal muscle fibers.²³ Appropriate biodistribution studies, determining the histotypes targeted by the co-i.v./i.c.v. delivery of AAV10, will enable the identification of the specific cell populations responsible for the therapeutic effect. This will be possible in the immediate future, taking advantage of a tagged AAV10-U7-hSOD1 co-expressing the AS molecules and a reporter gene.

Unlike chemically modified ASOs, for which the short lifetime requires their regular re-injection and which can cause toxicity,^{7,29} our AAV-U7 strategy to deliver AS molecules allows sustained therapeutic effects in injected animals and reduction of neuroinflammatory signs. The loco-regional delivery of an AAV-U7-mediated exon skipping approach is currently in clinical development for the restoration of truncated dystrophin in patients with Duchenne muscular dystrophy, and the first preclinical results showed a good safety profile in large animals.^{30,31} The therapeutic effect observed in our study could also be due to the high AAV dose used (4.5×10^{14} vg/kg), initially tested in proof of concept studies in newborn mice and then scaled up in adult mice. Indeed, thanks to the combination of the two delivery routes (i.c.v. and i.v.), it was possible to inject larger AAV quantities compared to studies in which the two delivery routes were used independently. Dose-finding studies will be necessary to determine the optimal AAV dosage for the translation of this therapy in large animals before translation to humans. Results from both preclinical and clinical studies showed that higher doses allow better therapeutic effects in neuromuscular disorders (C. Le Guiner, personal communication; J.R. Mendell et al., 2016, Am. Soc. Gene Cell Ther., conference),³² but difficulties to manufacture high vector doses and potential immunotoxicity remain obstacles to overcome the development of whole-body rescue strategies.

The efficacy and the clinical feasibility of our innovative SOD1-silencing approach highlights its considerable and realistic potential for ALS treatment, although some concerns regarding safety and the regulatory process of the combined central and peripheral mode of AAV delivery should be considered. The therapeutic translation of this strategy could thus benefit from a direct comparison of the three administration routes, namely, i.v., i.c.v., and co-i.v./i.c.v., using equal AAV doses. This will imply the injection of highly concentrated AAV productions to respect the volume limitations in brain ventricles compared to those of the bloodstream.

The use of AAV in clinical and preclinical studies has demonstrated transgene expression for several years.^{33,34} Furthermore, to prolong the AAV-mediated therapeutic effect, different strategies are currently developed to allow vector re-administration and escape to the immune response, such as exosome-embedded AAVs³⁵ or the use of tolerogenic nanoparticles.³⁶ In our study, we appreciated the prolonged AAV-mediated effect on hSOD1 mRNA at the end stage of treated animals (more than 250 days), although the major part of treated animals died developing progressive signs of limb paralysis. This finite therapeutic effect observed in treated SOD1^{G93A} mice is likely due to the accumulation of a residual amount of protein produced by the unskipped mRNA, attributable to the described prion-like properties of mutant hSOD1.^{37,38} Complete SOD1 suppression could be achieved by combining several U7-AS cassettes, as recently described by Schümperli and colleagues³⁹ for SMA or by coupling other methods to suppress SOD1, such as RNA interference or single chain antibodies⁴⁰ counteracting protein aggregation.

One-third of treated mice died from atypical ALS, without any sign of classical limb paralysis, rather showing a weight loss phenotype without ambulatory alterations, similar to the phenotype described by Stoica et al.¹³ This variability within the treated group could be due to stochastic distribution of the vector, which could have preferentially preserved limb motor units for yet unknown reasons.

The antisense sequences injected in SOD1^{G93A} mice were able to specifically silence hSOD1, without affecting endogenous SOD1 levels, thanks to the presence of ten mismatches between the human and mouse sequences. Such discrimination will not be possible in man because the described exon-skipping method will not distinguish between the product of the mutant or WT allele. Consequently, hSOD1 exon skipping could be virtually applied to all patients with SOD1 mutations, demonstrating SOD1 accumulation. Whether the partial knockdown of functional SOD1 is detrimental to normal cellular physiology is still a controversial matter.⁴¹ SOD1 knockout mice do not develop evident pathological phenotypes,⁴² and the first clinical trial using infused ASO against total hSOD1 has proven safe.⁷ The use of *in vitro* models, such as induced pluripotent stem-cell-derived motor neurons,⁴³ could help in the identification of potential toxic manifestations after such treatment. Moreover, a possible therapeutic solution to solve this problem would be to co-administer with the AAV10-U7-hSOD1, an antisense-resistant SOD1 coding sequence.

Interestingly, AAV10-U7-mediated exon 2 skipping mimicked a natural event observed in a Canadian SOD1-linked ALS family, carrying a heterozygous or homozygous deletion in a specific ESE sequence of SOD1 E2.⁴⁴ In this family, natural skipping of E2 reduced transcription of the mutant SOD1 allele, explaining the low penetrance of the mutation. This mutation was found in ALS patients or carriers who had low levels of toxic hSOD1 protein and were either weakly affected or unaffected.⁴⁴ In these patients, an exon 3 skipped form, which was never detected in our experiments, was observed.

When we tested the ASO *in vitro*, we observed some variability in exon-skipping efficacy. In some experiments, such as in the one shown in Figure S1B, the ΔE hSOD1 mRNA was much more evident in ASO2-treated cells relative to ASO1-treated cells. The thorough qPCR analysis on total mRNA levels (Figure 1B) showed a major efficacy in reducing the full-length RNA by the ASO1 sequence that was chosen for *in vivo* testing. One possible explanation for the lack of correspondence between the presence of the skipped form and the full-length hSOD1 mRNA reduction could involve other mechanisms than nonsense-mediated decay, such as nuclear RNA surveillance pathways for decay, as described by Ward et al.¹⁴ in the example of STAT3 exon skipping.

To evaluate SOD1 knockdown, we used an antibody recognizing the N-terminal region of the human SOD1 protein. The specific epitope is unknown and could detect some amino acids within exon 2. In this case, the effect on the protein would be attributed to the lack of a specific portion of the protein rather than to total suppression of hSOD1 protein. To corroborate the observed effect on protein suppression,

we performed western blot analysis with an antibody raised against the full recombinant protein and confirmed the SOD1 suppression of the total protein in AAV10-U7-hSOD1-injected mice (Figure S10).

Different studies have suggested the involvement of WT SOD1 misfolding in sporadic ALS,^{22,45,46} but this involvement was not confirmed by one recently published study.⁴⁷ Thus, the therapeutic application of AAV10-U7-mediated exon skipping may not be limited to the 12% of fALS patients who present with SOD1 mutations, but may also be applicable to some sporadic patients when hSOD1 accumulation is confirmed. This gene-silencing strategy could further be applied to a number of neurological disorders caused by “gain-of-function” gene mutations. In particular, because an U7-AS therapy has been demonstrated to be effective in the context of a trinucleotide repeat expansion pathology, namely Myotonic dystrophy type 1,⁴⁸ we can speculate that it could be further applied to other diseases cause by repeated nucleotide expansion and in particular to another form of ALS not linked to SOD1, the most common form of dominantly inherited ALS linked to C9orf72 mutations⁴⁹ caused by hexanucleotide repeat expansion.

MATERIALS AND METHODS

Animals

Animals were maintained following the European guidelines for the care and use of experimental animals and approved by the Charles Darwin N.5 Ethics Committee on Animal Experiments (agreement number 04830.02). High copy SOD1^{G93A} mice, B6SJL-Tg (SOD1^{G93A})1Gur/J (JACKSON SN 2726⁵⁰), were purchased from Jackson Laboratory. The *Colony Management Considerations* published in “Working with ALS Mice” were taken into account for the maintenance of the strain. SOD1^{G93A} mice were genotyped by PCR and assessed for hSOD1 genome copy number. To take into account the effect of gender on disease progression,⁵¹ sex-balanced groups of animals were injected.

AON Design

ESE finder 3.0 software⁵² was used to determine the ESEs in E2 of hSOD1. This software can predict binding sites for the most abundant SR proteins (SF2/ASF, IgM-BRCA1, SC35, SRp40, and SRp55). The consensus sequence for the SA was identified in the first hSOD1 intron. Five RNA-based ASOs masking these sequences on hSOD1 pre-mRNA were rationally designed. The ASOs were designed following the specific rules published by Artsma-Rus et al.⁵³ and using the RNAstructure 5.3 software. Each ASO was designed to be 20 nt long and to have the highest melting temperature (Tm) and the highest binding energy between the ASO and the target E2 sequence. ASO 1: 5'-CCACACCUUCACUG GUCCA-3'; ASO 2: 5'-GGCCUUCAGUCAGGUCCUUUA-3'; ASO 3: 5'-CUGGUCCAUUACUUUCUUU-3'; ASO 4: 5'-CCAUGCAG GCCUUCAGUCAG-3'; and ASO 5: 5'-CUGCUGUAUUAUCUCA AAC-3'. A scrambled ASO sequence was also selected as a negative control (ASO-CTR: 5'-GCUCAUUCGCUUCAUUCUU-3').

Cell Transfections

HEK293T cells were cultured in DMEM containing 10% fetal bovine serum (FBS) and 1% penicillin/streptomycin at 37°C in 5% CO₂ and

2'-O-methyl phosphorothioate (2'OMePS) ASOs were purchased from Eurogentec and re-suspended in H₂O RNase-free water at a final concentration of 1 µg/µL. Cells were transfected with 5 µg of each ASO with Oligofectamine (Invitrogen) following the manufacturer's instructions. The cells were harvested, 48 hr after transfection, for RNA extraction.

AAV Productions

The DNA sequences corresponding to the two best-performing ASOs were juxtaposed and cloned into pAAVsc_U7DTex23 (kindly provided by GENETHON) using PCR-mediated mutagenesis, as previously described.²⁰ The scAAV serotype 10 vectors were produced using the tri-transfection method, as described in Dominguez et al.⁵⁴ Vector titers were determined by qPCR on ITRs and expressed as vg/mL.

AAV Injections

SOD1^{G93A} mice of 50 days of age were used for direct injection into the lumbar spinal cord. Mice were anesthetized by an intraperitoneal injection of a ketamine/xylazine mixture (100 mg/kg ketamine and 10 mg/kg xylazine; 0.1 mL per 20 g of body weight). Injections were performed as reported by Raoul et al.⁸, and a total volume of 10 µL (two sites, 5 µL per site) containing 9.5×10^{10} vg (4.7×10^{12} vg/kg) of each vector was injected *per* mouse.

Combined i.c.v. and i.v. injections were performed in newborn mice with a total of 7.8×10^{11} vg (4.5×10^{14} vg/kg). Each mouse was injected with 70 µL of vector solution in the temporal vein and 10 µL in the lateral ventricles (unilateral injection, coordinates: -1 mm anterior-posterior, ± 1mm medio-lateral, and -1 mm dorso-ventral from bregma) using a Hamilton syringe (32G and 30-mm length needle).

A total of 7.8×10^{12} vg (4.5×10^{14} vg/kg) was administered to 50-day-old adult mice using the combined i.c.v. and i.v. delivery route. A roughly 20 µL viral suspension was stereotactically injected into the lateral ventricles (-0.2 mm anterior-posterior, ± 1 mm medio-lateral, and -1.8 mm dorso-ventral from bregma). An average of 320 µL of viral solution was injected into the tail vein or the retrobulbar sinus using an insulin syringe (29G, Terumo).

RT-PCR and qPCR Analyses

For *in vivo* analyses of mRNA levels, animals were anesthetized by intraperitoneal injection of ketamine (200 mg/kg, Imalgene, Merial) and xylazine (20 mg/kg, Rompun 2%, Bayer) at 112 days of age or at the end stage and transcardially perfused with PBS. Tissues (spinal cord, skeletal muscle, forebrain, brain stem, cerebellum, liver, and heart) were removed, snap frozen in liquid nitrogen, and stored at -80°C.

Total RNA was extracted either from frozen tissues or transfected HEK293 cells using the NucleoSpin RNA II RNA extraction kit (Macherey-Nagel) and quantified with a DeNovix DS-11 spectrophotometer.

For RT-PCR analyses, cDNA was synthesized from 1 µg of total RNA using oligo (dT) and random hexamer primers, according to the

iScript cDNA Synthesis kit protocol (Bio-Rad). E2 skipping in the hSOD1 mRNA was revealed by RT-PCR analysis of 200 ng of cDNA using the following primers (Eurogentec):

Primer Fw1, matching the hSOD1 exon 1: 5'-CTAGCGAGT TATGGCGAC-3';

Primer Rev 4/5, matching the hSOD1 exon 4-exon 5 boundary: 5'-GCCAATGATGCAATGGTCTC-3'.

For qRT-PCR (qPCR) analyses, cDNA was synthesized from 200 ng of RNA using the High Capacity cDNA RT Kit (Life Technologies) following the manufacturer's instructions. Amplified cDNA (30 ng) was mixed with 10 µL of Taqman Universal PCR Master Mix II - 2X (Life Technologies) and 1 µL of FAM probe for hSOD1 (TaqMan Gene expression assay Hs00533490m1, Life Technologies). For *in vitro* studies, 1 µL of VIC probe for human glyceraldehyde 3-phosphate dehydrogenase (GAPDH) (Taqman Gene expression assay Hs03929097_g1, Life Technologies) was used as endogenous control, and for *in vivo* analysis, 1 µL of VIC probe for mouse hypoxanthine-guanine phosphoribosyltransferase (HPRT) (Taqman gene expression assay Mm00446968_m1, Life Technologies) was used as endogenous control. Each sample was deposited in triplicate in a 96-well plate (Applied Biosystems). The thermal cycling conditions were: 1 min at 60°C and 10 min at 95°C, followed by 39 cycles of 15 s at 95°C and 1 min at 60°C in the StepOne Plus Real Time PCR System (Applied Biosystems).

The relative quantity of hSOD1 mRNA was calculated using the delta Ct/delta Ct method, taking into account the PCR signal of the target gene transcript of each sample (normalized to the endogenous control) relative to that of the control sample. The qPCR analyses were performed with the StepOne software v2.3 (Life Technologies).

Western Blot Analyses

Protein extracts from cells or freshly frozen tissues (see above) were prepared using a lysis buffer (150 mM NaCl, 50 mM Tris-HCl, 0.5% sodium deoxycholate, 1% NP40, and 0.1% SDS) supplied with a protease inhibitor cocktail (Complete Mini, Roche Diagnostics). Protein lysates were quantified using the DC protein assay kit (BioRad). 15-µg proteins (except for western blot in Figure S4) were separated on a 12% polyacrylamide gel (Criterion XT 12% bis-Tris, Bio-Rad) and analyzed by western blot using anti-α-tubulin (T5168, Sigma-Aldrich), anti-actin (A2066, Sigma-Aldrich), anti-human SOD1 (sc-8636, Santa Cruz Biotechnology), and anti-human SOD1 (556360, BD Pharmingen) antibodies. Peroxidase-conjugated mouse (VWR), rabbit (VWR), or goat (Life Technologies) immunoglobulin (Ig) antisera were used as secondary antibodies. Western blots were developed using the SuperSignal West Dura kit (Life Technologies), and densitometric analyses were performed using ImageJ software.

Histological Analyses and Microscopy

Animals were anesthetized by intraperitoneal injection of ketamine (100 mg/kg, Imalgene, Merial) and xylazine (10 mg/kg, Ronpun

2%, Bayer) at 112 days of age or at the end stage and transcardially perfused with PBS. The TA and *gastrocnemius* muscles were removed and perpendicularly or horizontally, respectively, placed on a cork support with tragacanth, frozen in cold isopentane, and stored at -80°C . Mice were then perfused with 4% paraformaldehyde (PFA) (Sigma-Aldrich) in PBS. The spines were explanted and stored in 4% PFA at $+4^{\circ}\text{C}$ for at least 24 hr, then transferred into a PBS-sucrose solution (30%) and stored for at least 24 hr at 4°C . Spinal cords were extracted, embedded in Tissue-Tek (OCT; Sakura Finetek), and frozen in cold isopentane (between -45°C and -50°C). 14- μm -thick sections were serially cut from the whole spinal cord at -22°C .

8- μm -thick cryosections were serially cut from TA muscles using a cryostat (Leica Microsystems) at -24°C , starting from the proximal origin, and stored at -80°C . Cryosections were fixed with 4% PFA and permeabilized in 0.1% Triton X-100 in PBS. Only spinal cord sections were also subjected to antigen retrieval with citrate buffer (10 mM citric acid, pH 6) at 85°C . Non-specific epitopes were blocked in a solution containing 5% BSA (IgG free, protease free, Jackson Laboratory), 0.1% Triton X-100 and 10% normal donkey serum (Millipore) (for ChAT), 10% normal goat serum (Life Technologies) (for GFAP, Iba1, hSOD1, and Laminin), or 1% FBS (Life Technologies) (for IIa-MHC) in PBS. The following primary antibodies were used in the corresponding blocking solution overnight at $+4^{\circ}\text{C}$: goat anti-ChAT (1:50; AB144P); rabbit anti GFAP (1:250; Dako #Z033401); rabbit anti-Iba1 (1:400, Wako #019-19741,); mouse anti-hSOD1 (1:100, BD Pharmigen #556360), rabbit anti-Laminin (1:400; Sigma-Aldrich #L9393), and mouse anti-MHC-IIa (undiluted SC-71, DSHB #AB2147165). After washing, tissues were incubated with the appropriate fluorescent-conjugated secondary antibodies: donkey anti-goat 488 (1:750, Life Technologies # A-11055, for ChAT), goat anti-rabbit 488 (1:750, Life Technologies # A-11008, for GFAP, Iba1, and Laminin), goat anti-mouse 594 (1:200, Life Technologies # A-11005 for hSOD1), or goat anti-mouse Cy3 (1:400, Jackson #115165206 for MHC-IIa), combined with DAPI staining (1:5,000, Sigma-Aldrich). Slides were mounted with FluoroMount-G Mounting Medium (Interchim).

Skeletal muscle images were obtained using an epifluorescence microscope (Leica Camera AG), digitized with a Nikon camera, and acquired using MetaMorph software. Spinal cord images were obtained using a Leica SPE confocal microscope (Leica Camera AG). Photographs were contrast enhanced by applying the brightness/contrast regulation of the Photoshop CS 8.0 software (Macintosh version, Adobe). Double immunofluorescence images were obtained by superimposing two or three single-color images of the same field.

ChAT-positive motor neurons (with a diameter $>20 \mu\text{m}$) were manually counted in the ventral horn of the cervical, thoracic, and lumbar spinal cord segments using an epifluorescence microscope (Leica Camera AG). Astroglial activation was evaluated by measuring the fluorescence intensity of the GFAP staining in the gray matter of the spinal cords using ImageJ software. Microglial activation was evaluated by counting the Iba-1-positive cells in the gray matter of spinal

cord sections. The myofiber area and number were quantified using ImageJ software. Fiber areas were calculated in square pixels and then converted into μm^2 . Cell counting and morphological analyses were performed in a blinded manner.

NMJ Analysis

For whole-mount staining of the EDL muscles, the protocol described in the SOP SMA.M_1.2.003 of “Treat-NMD neuromuscular network” was used with slight modifications. EDL muscles were freshly explanted, washed in PBS, and incubated on a rotating shaker (Stuart rotator SB3) for 10 min in a solution containing 500 $\mu\text{g}/\mu\text{L}$ of 594-conjugated BTX (Life Technologies # B-13423) in PBS. After PBS washings, muscles were fixed with 4% PFA in PBS for 15 min and dissected under a stereomicroscope (Zeiss). Non-specific epitopes were blocked in a solution containing 5% BSA, 0.1% Triton X-100, and 10% normal goat serum for 30 min. The monoclonal antibody anti-NF (1:200, MAB5254) was incubated overnight at $+4^{\circ}\text{C}$. After washings, EDL muscles were incubated with goat anti-mouse 488 (1:200, Life Technologies A-21121) and mounted on slides with FluoroMount-G.

20- μm -thick cryosections were serially cut from *gastrocnemius* muscles using a cryostat at -24°C and stored at -80°C . Sections were fixed with cold acetone, incubated with 594-conjugated BTX, and then processed for anti-NF immunofluorescence, as described above.

Fluorescence images along the z axis were taken by a Leica SPE confocal microscope. Z stacks were done using ImageJ software, and images were processed as described above. Endplates were scored as innervated when BTX and NF signals co-localized and were scored as denervated if they showed only BTX staining. Endplate areas were measured using ImageJ software and were calculated in square pixels and then converted into μm^2 .

Analyses of Muscle Contractile Properties

Absolute maximal force, specific maximal force, and maximal activation capacity were evaluated by measuring the *in situ* isometric muscle contraction of the TA in response to nerve stimulation (as described by Ferry et al.⁵⁵). Mice were anesthetized by intraperitoneal administration of a pentobarbital solution (60 mg/kg). The knee and foot were fixed with clamps and stainless steel pins, and the distal tendon of the TA muscle was attached to an isometric transducer, dual-mode lever (Aurora Scientific) using a silk ligature, under constant tension. Force responses to muscle and nerve electrical stimulation (square wave pulses of 0.1-ms duration, pulse frequency of 75–150 Hz, and stimulation train of 500 ms) were successively recorded. Absolute maximal isometric force was determined at optimal length (length at which maximal tension was obtained during the tetanus) and then normalized to the muscle mass to estimate specific maximal force. We also compared the maximal tetanic force produced following stimulation of either the sciatic nerve or the muscle directly. If neuromuscular transmission is impaired, indirect muscle stimulation would be expected to produce lower maximal tetanic

force values than when the muscle is stimulated via the nerve. In this study, we used this comparison as a functional index of the capacity of the neuromuscular transmission to maximally activate the muscle (maximal activation capacity).

Behavioral Analyses

Body weight, strength, motor coordination, and spontaneous activity were assessed twice a week. The grip strength of the four limbs was evaluated using a grip strength meter (Biobest) to determine the peak force (in grams) generated when the mouse is pulled back from a metal gird. For each test, five measures per animal were recorded. Motor coordination was assessed using an accelerating rotarod instrument (Biobest), starting at 4 rpm/min. The time spent on the rotarod before falling was recorded in two runs per animal. At 17 weeks of age, the spontaneous activity of mice was assessed overnight (12 hr) using an actimeter to record the number of crossed infrared light beams, and data were analyzed using Track software (Biobest).

Survival was determined as the time when the mouse was unable to right itself in 30 s when placed on its side (defined as the end stage).

Statistical Analyses

Statistical significance was assessed using the Student's paired t test, one-way ANOVA, or two-way ANOVA, depending on the experimental protocols, as stated in the figure legends. Survival and disease-onset curves were compared using the log-rank Mantel-Cox test. Results were considered to be significant for p values under 0.05. All statistical tests were performed using Prism software (version 4.0, GraphPad). The therapeutic study of AAV-U7-hSOD1 delivery in adult SOD1^{G93A} mice was designed following the *Prize4Life* criteria and the recommendations published by Scott et al.⁵⁶

SUPPLEMENTAL INFORMATION

Supplemental Information includes ten figures and one movie and can be found with this article online at <http://dx.doi.org/10.1016/j.ymthe.2017.05.017>.

AUTHOR CONTRIBUTIONS

M.G.B. and M.B. planned, designed, interpreted the experiments, and wrote the manuscript. T.V. intellectually contributed to the study and supervised the revision process. M.G.B., M.C.-T., C.B., and A.C. carried out experiments. M.G.B., M.R., B.G., and T.M. maintained the animals and performed behavioral analyses and injections. M.C.-T. and S.A. produced the AAV vectors. A.F. performed the electrophysiological analyses.

CONFLICTS OF INTEREST

The authors declare no competing financial interests.

ACKNOWLEDGMENTS

The authors sincerely thank Bruno Cadot (Center of Research in Myology) for his help in microscopy image acquisition, Yannick Tanguy for taking the mouse photographs and help in the statistical

analyses, Aurore Besse for her technical assistance, and Ilaria Di Emidio for the illustrations. We also thank G. Haase and M. Crescenzi for critical reading of the manuscript. This work was funded by the Association Française contre les Myopathies (AFM), the University Pierre et Marie Curie (UPMC), the Institut National de la Santé et de la Recherche Médicale (INSERM), the Centre National de la Recherche Scientifique (CNRS), the Association Institut de Myologie (AIM), the Otto per Mille Waldensian Church, and the Association pour la Recherche sur la Sclérose Latérale Amyotrophique (ARSLA). T.V. is supported by the NIHR GOSH Biomedical Research Centre.

REFERENCES

- Pasinelli, P., and Brown, R.H. (2006). Molecular biology of amyotrophic lateral sclerosis: insights from genetics. *Nat. Rev. Neurosci.* **7**, 710–723.
- Bensimon, G., Lacomblez, L., and Meininger, V.; ALS/Riluzole Study Group (1994). A controlled trial of riluzole in amyotrophic lateral sclerosis. *N. Engl. J. Med.* **330**, 585–591.
- Renton, A.E., Chiò, A., and Traynor, B.J. (2014). State of play in amyotrophic lateral sclerosis genetics. *Nat. Neurosci.* **17**, 17–23.
- Rosen, D.R., Siddique, T., Patterson, D., Figlewicz, D.A., Sapp, P., Hentati, A., Donaldson, D., Goto, J., O'Regan, J.P., Deng, H.X., et al. (1993). Mutations in Cu/Zn superoxide dismutase gene are associated with familial amyotrophic lateral sclerosis. *Nature* **362**, 59–62.
- Scarrott, J.M., Herranz-Martín, S., Alraifah, A.R., Shaw, P.J., and Azzouz, M. (2015). Current developments in gene therapy for amyotrophic lateral sclerosis. *Expert Opin. Biol. Ther.* **15**, 935–947.
- Smith, R.A., Miller, T.M., Yamanaka, K., Monia, B.P., Condon, T.P., Hung, G., Lobsiger, C.S., Ward, C.M., McAlonis-Downes, M., Wei, H., et al. (2006). Antisense oligonucleotide therapy for neurodegenerative disease. *J. Clin. Invest.* **116**, 2290–2296.
- Miller, T.M., Pestronk, A., David, W., Rothstein, J., Simpson, E., Appel, S.H., Andres, P.L., Mahoney, K., Allred, P., Alexander, K., et al. (2013). An antisense oligonucleotide against SOD1 delivered intrathecally for patients with SOD1 familial amyotrophic lateral sclerosis: a phase 1, randomised, first-in-man study. *Lancet Neurol.* **12**, 435–442.
- Raoul, C., Abbas-Terki, T., Bensadoun, J.C., Guillot, S., Haase, G., Szulc, J., Henderson, C.E., and Aebsicher, P. (2005). Lentiviral-mediated silencing of SOD1 through RNA interference retards disease onset and progression in a mouse model of ALS. *Nat. Med.* **11**, 423–428.
- Ralph, G.S., Radcliffe, P.A., Day, D.M., Carthy, J.M., Leroux, M.A., Lee, D.C., Wong, L.F., Bilsland, L.G., Greensmith, L., Kingsman, S.M., et al. (2005). Silencing mutant SOD1 using RNAi protects against neurodegeneration and extends survival in an ALS model. *Nat. Med.* **11**, 429–433.
- Foust, K.D., Salazar, D.L., Likhite, S., Ferraiuolo, L., Ditsworth, D., Ilieva, H., Meyer, K., Schmelzer, L., Braun, L., Cleveland, D.W., et al. (2013). Therapeutic AAV9-mediated suppression of mutant SOD1 slows disease progression and extends survival in models of inherited ALS. *Mol. Ther.* **21**, 2148–2159.
- Wang, H., Yang, B., Qiu, L., Yang, C., Kramer, J., Su, Q., Guo, Y., Brown, R.H., Jr., Gao, G., and Xu, Z. (2014). Widespread spinal cord transduction by intrathecal injection of rAAV delivers efficacious RNAi therapy for amyotrophic lateral sclerosis. *Hum. Mol. Genet.* **23**, 668–681.
- Borel, F., Gernoux, G., Cardozo, B., Metterville, J.P., Toro Cabreja, G.C., Song, L., Su, Q., Gao, G.P., Elmallah, M.K., Brown, R.H., Jr., et al. (2016). Therapeutic rAAVrh10-mediated SOD1 silencing in adult SOD1(G93A) mice and nonhuman primates. *Hum. Gene Ther.* **27**, 19–31.
- Stoica, L., Todeasa, S.H., Cabrera, G.T., Salameh, J.S., ElMallah, M.K., Mueller, C., Brown, R.H., Jr., and Sena-Esteves, M. (2016). Adeno-associated virus-delivered artificial microRNA extends survival and delays paralysis in an amyotrophic lateral sclerosis mouse model. *Ann. Neurol.* **79**, 687–700.

14. Ward, A.J., Norrbom, M., Chun, S., Bennett, C.F., and Rigo, F. (2014). Nonsense-mediated decay as a terminating mechanism for antisense oligonucleotides. *Nucleic Acids Res.* **42**, 5871–5879.
15. Chang, Y.F., Imam, J.S., and Wilkinson, M.F. (2007). The nonsense-mediated decay RNA surveillance pathway. *Annu. Rev. Biochem.* **76**, 51–74.
16. Cartegni, L., Chew, S.L., and Krainer, A.R. (2002). Listening to silence and understanding nonsense: exonic mutations that affect splicing. *Nat. Rev. Genet.* **3**, 285–298.
17. Nagy, E., and Maquat, L.E. (1998). A rule for termination-codon position within intron-containing genes: when nonsense affects RNA abundance. *Trends Biochem. Sci.* **23**, 198–199.
18. Yoo, B.H., Bochkareva, E., Bochkarev, A., Mou, T.C., and Gray, D.M. (2004). 2'-O-methyl-modified phosphorothioate antisense oligonucleotides have reduced non-specific effects in vitro. *Nucleic Acids Res.* **32**, 2008–2016.
19. Schümperli, D., and Pillai, R.S. (2004). The special Sm core structure of the U7 snRNP: far-reaching significance of a small nuclear ribonucleoprotein. *Cell. Mol. Life Sci.* **61**, 2560–2570.
20. Goyenvalle, A., Vulin, A., Fougerousse, F., Leturcq, F., Kaplan, J.C., Garcia, L., and Danos, O. (2004). Rescue of dystrophic muscle through U7 snRNA-mediated exon skipping. *Science* **306**, 1796–1799.
21. Piétri-Rouxel, F., Gentil, C., Vassilopoulos, S., Baas, D., Mouisel, E., Ferry, A., Vignaud, A., Hourdé, C., Marty, I., Schaeffer, L., et al. (2010). DHPR alpha1S subunit controls skeletal muscle mass and morphogenesis. *EMBO J.* **29**, 643–654.
22. Haidet-Phillips, A.M., Hester, M.E., Miranda, C.J., Meyer, K., Braun, L., Frakes, A., Song, S., Likhite, S., Murtha, M.J., Foust, K.D., et al. (2011). Astrocytes from familial and sporadic ALS patients are toxic to motor neurons. *Nat. Biotechnol.* **29**, 824–828.
23. Dobrowolny, G., Aucello, M., Rizzuto, E., Beccafico, S., Mammucari, C., Boncompagni, S., Belia, S., Wannenes, F., Nicoletti, C., Del Prete, Z., et al. (2008). Skeletal muscle is a primary target of SOD1G93A-mediated toxicity. *Cell Metab.* **8**, 425–436.
24. Boillée, S., Vande Velde, C., and Cleveland, D.W. (2006). ALS: a disease of motor neurons and their nonneuronal neighbors. *Neuron* **52**, 39–59.
25. Talmadge, R.J. (2000). Myosin heavy chain isoform expression following reduced neuromuscular activity: potential regulatory mechanisms. *Muscle Nerve* **23**, 661–679.
26. Peggion, C., Massimino, M.L., Biancotto, G., Angeletti, R., Reggiani, C., Sorgato, M.C., Bertoli, A., and Stella, R. (2017). Absolute quantification of myosin heavy chain isoforms by selected reaction monitoring can underscore skeletal muscle changes in a mouse model of amyotrophic lateral sclerosis. *Anal. Bioanal. Chem.* **409**, 2143–2153.
27. Vinsant, S., Mansfield, C., Jimenez-Moreno, R., Del Gaizo Moore, V., Yoshikawa, M., Hampton, T.G., Prevette, D., Caress, J., Oppenheim, R.W., and Milligan, C. (2013). Characterization of early pathogenesis in the SOD1(G93A) mouse model of ALS: part I, background and methods. *Brain Behav.* **3**, 335–350.
28. Vinsant, S., Mansfield, C., Jimenez-Moreno, R., Del Gaizo Moore, V., Yoshikawa, M., Hampton, T.G., Prevette, D., Caress, J., Oppenheim, R.W., and Milligan, C. (2013). Characterization of early pathogenesis in the SOD1(G93A) mouse model of ALS: part II, results and discussion. *Brain Behav.* **3**, 431–457.
29. Frazier, K.S. (2015). Antisense oligonucleotide therapies: the promise and the challenges from a toxicologic pathologist's perspective. *Toxicol. Pathol.* **43**, 78–89.
30. Vulin, A., Barthélémy, I., Goyenvalle, A., Thibaud, J.L., Beley, C., Griffith, G., Benchaouir, R., le Hir, M., Unterfinger, Y., Lorain, S., et al. (2012). Muscle function recovery in golden retriever muscular dystrophy after AAV1-U7 exon skipping. *Mol. Ther.* **20**, 2120–2133.
31. Le Guiner, C., Montus, M., Servais, L., Cherel, Y., Francois, V., Thibaud, J.L., Wary, C., Matot, B., Larcher, T., Guigand, L., et al. (2014). Forelimb treatment in a large cohort of dystrophic dogs supports delivery of a recombinant AAV for exon skipping in Duchenne patients. *Mol. Ther.* **22**, 1923–1935.
32. Mack, D.L., Poulard, K., Goddard, M.A., Latournerie, V., Snyder, J.M., Grange, R.W., Elverman, M.R., Denard, J., Veron, P., Buscaro, L., et al. (2017). Systemic AAV8-mediated gene therapy drives whole-body correction of myotubular myopathy in dogs. *Mol. Ther.* **25**, 839–854.
33. Buchlis, G., Podskaloff, G.M., Radu, A., Hawk, S.M., Flake, A.W., Mingozi, F., and High, K.A. (2012). Factor IX expression in skeletal muscle of a severe hemophiliac patient 10 years after AAV-mediated gene transfer. *Blood* **119**, 3038–3041.
34. Nathwani, A.C., Reiss, U.M., Tuddenham, E.G., Rosales, C., Chowdary, P., McIntosh, J., Della Peruta, M., Lheriteau, E., Patel, N., Raj, D., et al. (2014). Long-term safety and efficacy of factor IX gene therapy in hemophilia B. *N. Engl. J. Med.* **371**, 1994–2004.
35. Hudry, E., Martin, C., Gandhi, S., György, B., Scheffer, D.I., Mu, D., Merkel, S.F., Mingozi, F., Fitzpatrick, Z., Dimant, H., et al. (2016). Exosome-associated AAV vector as a robust and convenient neuroscience tool. *Gene Ther.* **23**, 819.
36. Kishimoto, T.K., Ferrari, J.D., LaMothe, R.A., Kolte, P.N., Griset, A.P., O'Neil, C., Chan, V., Browning, E., Chalishazar, A., Kuhlman, W., et al. (2016). Improving the efficacy and safety of biologic drugs with tolerogenic nanoparticles. *Nat. Nanotechnol.* **11**, 890–899.
37. Chattopadhyay, M., Durazo, A., Sohn, S.H., Strong, C.D., Gralla, E.B., Whitelegge, J.P., and Valentine, J.S. (2008). Initiation and elongation in fibrillation of ALS-linked superoxide dismutase. *Proc. Natl. Acad. Sci. USA* **105**, 18663–18668.
38. Ayers, J.I., Fromholt, S.E., O'Neal, V.M., Diamond, J.H., and Borchelt, D.R. (2016). Prion-like propagation of mutant SOD1 misfolding and motor neuron disease spread along neuroanatomical pathways. *Acta Neuropathol.* **131**, 103–114.
39. Odermatt, P., Trüb, J., Furrer, L., Fricker, R., Marti, A., and Schümperli, D. (2016). Somatic therapy of a mouse SMA model with a U7 snRNA gene correcting SMN2 splicing. *Mol. Ther.* **24**, 1797–1805.
40. Patel, P., Kriz, J., Gravel, M., Soucy, G., Bareil, C., Gravel, C., and Julien, J.P. (2014). Adeno-associated virus-mediated delivery of a recombinant single-chain antibody against misfolded superoxide dismutase for treatment of amyotrophic lateral sclerosis. *Mol. Ther.* **22**, 498–510.
41. Saccon, R.A., Bunton-Stasyshyn, R.K., Fisher, E.M., and Fratta, P. (2013). Is SOD1 loss of function involved in amyotrophic lateral sclerosis? *Brain* **136**, 2342–2358.
42. Reaume, A.G., Elliott, J.L., Hoffman, E.K., Kowall, N.W., Ferrante, R.J., Siwek, D.F., Wilcox, H.M., Flood, D.G., Beal, M.F., Brown, R.H., Jr., et al. (1996). Motor neurons in Cu/Zn superoxide dismutase-deficient mice develop normally but exhibit enhanced cell death after axonal injury. *Nat. Genet.* **13**, 43–47.
43. Nedelec, S., Onteniente, B., Peschanski, M., and Martinat, C. (2013). Genetically modified human pluripotent stem cells: new hopes for the understanding and the treatment of neurological diseases? *Curr. Gene Ther.* **13**, 111–119.
44. Zinman, L., Liu, H.N., Sato, C., Wakutani, Y., Maruelle, A.F., Moreno, D., Morrison, K.E., Mohlke, K.L., Bilbao, J., Robertson, J., et al. (2009). A mechanism for low penetrance in an ALS family with a novel SOD1 deletion. *Neurology* **72**, 1153–1159.
45. Bosco, D.A., Morfini, G., Karabacak, N.M., Song, Y., Gros-Louis, F., Pasinelli, P., Goolsby, H., Fontaine, B.A., Lemay, N., McKenna-Yasek, D., et al. (2010). Wild-type and mutant SOD1 share an aberrant conformation and a common pathogenic pathway in ALS. *Nat. Neurosci.* **13**, 1396–1403.
46. Forsberg, K., Jonsson, P.A., Andersen, P.M., Bergemalm, D., Graffmo, K.S., Hultdin, M., Jacobsson, J., Rosquist, R., Marklund, S.L., and Brännström, T. (2010). Novel antibodies reveal inclusions containing non-native SOD1 in sporadic ALS patients. *PLoS ONE* **5**, e11552.
47. Da Cruz, S., Bui, A., Saberi, S., Lee, S.K., Stauffer, J., McAlonis-Downes, M., Schulte, D., Pizzo, D.P., Parone, P.A., Cleveland, D.W., et al. (2017). Misfolded SOD1 is not a primary component of sporadic ALS. *Acta Neuropathol.* Published online February 28, 2017. <http://dx.doi.org/10.1007/s00401-017-1688-8>.
48. François, V., Klein, A.F., Beley, C., Jollet, A., Lemercier, C., Garcia, L., and Furling, D. (2011). Selective silencing of mutated mRNAs in DM1 by using modified hU7-snRNAs. *Nat. Struct. Mol. Biol.* **18**, 85–87.
49. Jiang, J., Zhu, Q., Gendron, T.F., Saberi, S., McAlonis-Downes, M., Seelman, A., Stauffer, J.E., Jafar-Nejad, P., Drenner, K., Schulte, D., et al. (2016). Gain of toxicity from ALS/FTD-linked repeat expansions in C9ORF72 is alleviated by antisense oligonucleotides targeting GGGGCC-containing RNAs. *Neuron* **90**, 535–550.
50. Gurney, M.E. (1994). Transgenic-mouse model of amyotrophic lateral sclerosis. *N. Engl. J. Med.* **331**, 1721–1722.
51. Pfohl, S.R., Halicek, M.T., and Mitchell, C.S. (2015). Characterization of the contribution of genetic background and gender to disease progression in the SOD1 G93A mouse model of amyotrophic lateral sclerosis: a meta-analysis. *J. Neuromuscul. Dis.* **2**, 137–150.
52. Cartegni, L., Wang, J., Zhu, Z., Zhang, M.Q., and Krainer, A.R. (2003). ESEfinder: a web resource to identify exonic splicing enhancers. *Nucleic Acids Res.* **31**, 3568–3571.

53. Aartsma-Rus, A., van Vliet, L., Hirschi, M., Janson, A.A., Heemskert, H., de Winter, C.L., de Kimpe, S., van Deutekom, J.C., 't Hoen, P.A., and van Ommen, G.B. (2009). Guidelines for antisense oligonucleotide design and insight into splice-modulating mechanisms. *Mol. Ther.* **17**, 548–553.
54. Dominguez, E., Marais, T., Chatauret, N., Benkhelifa-Ziyat, S., Duque, S., Ravassard, P., Carcenac, R., Astord, S., Pereira de Moura, A., Voit, T., et al. (2011). Intravenous scAAV9 delivery of a codon-optimized SMN1 sequence rescues SMA mice. *Hum. Mol. Genet.* **20**, 681–693.
55. Ferry, A., Joanne, P., Hadj-Said, W., Vignaud, A., Lilienbaum, A., Hourdé, C., Medja, F., Noirez, P., Charbonnier, F., Chatonnet, A., et al. (2014). Advances in the understanding of skeletal muscle weakness in murine models of diseases affecting nerve-evoked muscle activity, motor neurons, synapses and myofibers. *Neuromuscul. Disord.* **24**, 960–972.
56. Scott, S., Kranz, J.E., Cole, J., Lincecum, J.M., Thompson, K., Kelly, N., Bostrom, A., Theodos, J., Al-Nakhala, B.M., Vieira, F.G., et al. (2008). Design, power, and interpretation of studies in the standard murine model of ALS. *Amyotroph. Lateral Scler.* **9**, 4–15.